ARTICLE

The influence of structure on the methyl group dynamics of the polymorphic complexes: 6,6'-dimethyl-2,2'-dipyridyl with halo derivatives of benzoquinone acids

Received 00th January 20xx,
Accepted 00th January 20xx

DOI: 10.1039/x0xx00000x

Magdalena Rok[a], Marcin Moskwa[a], Przemysław Dopieralski[a], Wojciech Medycki[b], Michaela Zamponi[c], Grażyna Bator[a]

Recently, interest in organic ferroelectrics or antiferroelectrics representing a metal-free perovskite-type has increased significantly. This interest results from the properties of organic systems. First of all, they do not have toxic metals in their structure. Therefore they are environmentally friendly. Also, the method of preparation, simple syntheses, and low-temperature processability increase their attractiveness in terms of application. In this paper, the above properties are associated with the proton dynamics in organic donor-acceptor systems. We present the comparison of the physicochemical properties of four molecular complexes containing the proton acceptor molecule, 6,6'-dimethyl-2,2'-bipyridyl (66DMBP), and one of three organic acid molecules belonging to the benzoquinones group. As proton donor molecules the organic acids: chloranilic, bromanilic as well as iodanilic acids have been chosen. We present the results of experiments concerning the determination of the crystal structures, ^{1}H NMR, inelastic neutron scattering (INS) and UV/VIS spectra. In the theoretical part, we attempt to explain the influence of the crystallization method (a type of solvent) on *transoid* or *cisoid* arrangement of 66DMBP. In the theoretical approach, we focus on two forms of the complex with choranilic acid, α–66DMBP·CLA and β–66DMBP·CLA, which undergo solid-to-solid phase transitions, at 380 and 317 K, respectively. We have chosen these examples because the α analogue possesses the ferroelectric properties in a wide range of temperature.

1. Introduction

Understanding the role of stimuli controlling the crystallisation processes is a prime challenge for the design of novel materials for a potential application in modern electronics. Such knowledge allows us to predict the strength and types of specific interactions, like hydrogen bonds (HB), in the crystalline solid state. The aim is to investigate such complexes, in which the molecules may form strong and medium HBs. The interesting electrical properties appear as a result of the proton dynamics in the coupled HBs.

Here, we study organic molecular complexes formed by proton donors and acceptors. As the proton acceptor, we have chosen the methyl derivative of bipyridyl: 6,6'-dimethyl-2,2'-bipyridyl (66DMBP, pKa=5.2), as an intriguing precursor for the molecular complexes, in which even the weak hydrogen bonds have an effect on the material properties. This interest is strongly related to the molecular structure of the above-mentioned bipyridyl molecule. The molecule is built of two aromatic pyridine rings, which in principle can form planar *trans* or nonplanar *cis* conformation.[1,2] Depending on the conformation, both nitrogen atoms in 66DMBP can form hydrogen bonds on one or two sides of the molecule (see Fig. S1, ESI).

As a proton donor, the anilic acids (2,5-dihydroxy-p-benzoquinones, H_2X, X = Cl^-, Br^-, I^-) have been selected, which have an excellent proton donating property. One of the examples is the chloranilic acid (2,5-dichloro-3,6-dihydroxy-1,4-benzoquinone (chloranilic, CLA, pKa_1=0.76, pKa_2=3.08), which has two OH (hydroxyl) groups and two carbonyl groups (C=O). This means that in fact, CLA may be either a donor or an acceptor of protons. Such a structure allows creating an infinite supramolecular chain with hydrogen bonds.[3,4]

Depending on the path of synthesis (e.g. the type of solvent and temperature) the binary-compound crystals of 66DMBP·CLA can create three polymorphic forms of α–66DMBP·CLA, β–66DMBP·CLA or γ–66DMBP·CLA.[5,6] Two complexes, α–66DMBP·CLA and β–66DMBP·CLA, undergo one solid-to-solid phase transition at 380 and 317 K, respectively. While for γ–66DMBP·CLA form three-phase transitions were observed (202, 320 and 379 K), only in the case of the α– form, a ferroelectric to antiferroelectric transition appeared,

[a] Faculty of Chemistry, University of Wroclaw, 14 F. Joliot – Curie, 50-383 Wroclaw, Poland
[b] Institute of Molecular Physics, Polish Academy of Sciences, Smoluchowskiego 17, 60-179 Poznań, Poland
[c] Forschungszentrum Jülich GmbH, Jülich Centre for Neutron Science (JCNS) at Heinz Maier-Leibnitz Zentrum (MLZ), Lichtenbergstr. 1, 85748 Garching, Germany
† e-mail: magdalena.rok@chem.uni.wroc.pl

Electronic Supplementary Information (ESI) available: [details of any supplementary information available should be included here]. See DOI: 10.1039/x0xx00000x

which is very important, e.g. for organic electronics. The mechanism of the observed phenomena for α–66DMBP·CLA, ferroelectricity or electrical conductivity, are strongly connected with the proton dynamics in the hydrogen O–H···N and N^+–H···O^- bonds. We are searching for the crystals, in which the acid and base molecules are placed alternately, forming infinite chains with HBs in the solid-state. The ordered protons in the supramolecular polar chain at low temperature are the origin of the polar properties observed for these crystals. The non-ferroelectric β–66DMBP·CLA crystals also undergo structural rearrangements of protons through hydrogen bonds. These changes are not, however, related to the long-range interactions and in consequence, the β–form does not reveal any polar properties.

The rich polymorphism in the crystals described is primarily due to the synthesis method. The ferroelectric α form can be obtained only from the acetone solution, whereas β from more polar solvents (methanol, ethanol). The γ form demands low temperature (255 K) and the methanol solution. In this work, we focus our attention only on the α and β forms from the chloranilic group. Therefore, in the theoretical approach, we made calculations regarding the stabilisation of cis-trans conformations in solvents that differ in polarity (acetone, ethanol, methanol).

Moreover, our purpose in this work is to compare the properties of 66DMBP·CLA with those of the completely new complexes with either 2,5-dibromo-3,6-dihydroxy-1,4-benzoquinone (66DMBP·BRA) or 2,5-diiodo-3,6-dihydroxy-1,4-benzoquinone (66DMBP·IA). We carried out experiments concerning the determination of the crystal structures, ^{1}H NMR, inelastic neutron scattering (INS), UV/VIS spectra for the different compounds. We aim to find the explanation for the observed physicochemical properties of the compounds.

2. Experimental and computational details

2.1 Sample preparation

The single crystals of the molecular complexes: 6,6'-dimethyl-2,2'-bipyridyl (66DMBP, Sigma-Aldrich ≥ 98%)) with bromanilic acid (BRA, TCI > 98%) with stoichiometry 1:1 (66DMBP·BRA, **1**) and 2:1 (66DMBP·BRA, **2**) were grown from acetone and methanol solution, respectively. The complex of 66DMBP·IA (**3**) was prepared by mixing equimolar amounts of amine and iodanilic acid (IA). Iodanilic acid (IA) was prepared from p-chloranil, according to the literature[7]. The composition of the synthesised compounds was identified by elemental analysis using the Vario FT III Element Analyzer on C, H and N (% exp./theor.): C(44.32/44.84), H(2.48/2.93), N(5.67/5.81); C(54.07/54.20), H(3.923/3.51), N(8.41.16/8.32) and C(37.32/37.53), H(2.28/2.45), N(4.57/4.86) for 66DMBP·BRA (numbered as **1**), 66DMBP·BRA (2:1) (**2**) and 66DMBP·IA (**3**), respectively.

The compounds of α-66DMBP·CLA and β-66DMBP·CLA were prepared by mixing equimolar amounts of amine (Sigma-Aldrich ≥ 98%) and chloranilic acids (TCI > 98%) in acetone and methanol solution, respectively. The colour of α–form (elongated plates) was red, β–form (polygond) dark violet. Analysis on C, H and N (% exp./theor.): C(55.1/54.98), H(3.47/3.59), N(7.14/7.12) and C(55.0/54.98), H(3.81/3.59), N(7.17/7.12) for α-66DMBP·CLA and β-66DMBP·CLA, respectively.

2.2 UV/VIS spectra

UV/VIS spectra were recorded at room temperature on SP–880 (Metertech) in the range between 350 and 800 nm. The crystals of α-66DMBP·CLA were solved in acetone ($C=9.41\cdot10^{-4}$ mol/dm^3), the form β-66DMBP·CLA in methanol ($C=9.41\cdot10^{-4}$ mol/dm^3). The organic solvents: acetone (Sigma-Aldrich, for HPLC ≥99.9%) and methanol (Sigma-Aldrich, for HPLC ≥99.9%) were used without further purification.

2.3 X-ray diffraction analysis

Single-crystal X-ray diffraction data for **1**, **2** and **3** were collected on an Agilent Technologies Xcalibur, Ruby or KUMA KM4CCD *κ*-axis four-circle diffractometer equipped with an Oxford Cryosystem cooler using graphite monochromated MoKα radiation. The structure was solved by direct methods with the SHELXS-2014/7[8] program and refined by the full-matrix least-squares methods on all F^2 data using SHELXL-2014/7 (ref. [9]). Data collection was performed by using CrysAlis CCD; the reduction was executed on CrysAlis Pro.[10] All non-hydrogen atoms were refined anisotropically. H atoms attached to O and N atoms were found in a difference Fourier map. H atom isotropic temperature factors were assumed as 1.2 times U_{eq}(N), 1.5 times U_{eq}(O). In the complex **3** the O-bound and N-bound H atoms were refined with O–H, N–H distances restrained to 0.900(2) Å and were then constrained to ride on their parent atoms (AFIX 3 instruction in SHELXL-2014/7) [9]. H atoms attached to C were treated as a riding model and their isotropic temperature factors were assumed to be 1.2-times U_{eq} or 1.5-times U_{eq} for C atoms of methyl groups. The crystal data, together with the experimental and refinement details, are given in Table S1 (ESI). Crystallographic data for the structures reported in this paper (excluding structures factors) have been deposited with the CCDC No. 2009774-2009776.

2.4 Computational Methods and Details

The theoretical conformational analysis was performed on the 6,6'-dimethyl-2,2'-bipyridinium molecule and its cation protonated on one of the nitrogen atoms utilising two different approaches to include a solvent.

Static calculations

Using two different models (PCM[11,12] and COSMO[13]) together with B3LYP functional and cc-pVTZ[14] basis set, we were able to quickly estimate relative energies corresponding to different values of dihedral angle between atoms N-C-C-N, and thus to different conformations of the molecule. Calculations were performed in the gas phase and solvents: acetone, ethanol and methanol.

Dynamic calculations

Subsequently, we performed much advanced, ab initio molecular dynamics[15] simulations using the efficient Car-Parrinello[16] propagation scheme in two solvents: acetone (15 molecules) and methanol (37 molecules), which allowed us to include not only specific interactions between molecules (such as van der Waals interactions and hydrogen bonding) but also temperature effects

because all dynamical simulations were performed in the canonical ensemble at 295K, in contrary to static calculations which are performed by definition in 0 K. A more detailed description of computational methods can be found in ESI (Fig. S2).

2.5 Neutron spectroscopy

High-resolution neutron spectra were measured on the backscattering spectrometer SPHERES[17] operated by JCNS at the Heinz Maier-Leibnitz Zentrum (Garching, Germany) at temperatures between 3 and 40 K for the inelastic spectra and up to 200 K for the quasielastic spectra in the energy range up to ±30 μeV. The programs SLAW[18] and FRIDA[19] were used for reducing and fitting the data. A vanadium measurement was used to determine the instrumental resolution and for normalization. The momentum transfer (Q) range is 0.2-1.8 $Å^{-1}$, the inelastic spectra were integrated over the range of 0.6-1.66 $Å^{-1}$.

2.6 ^{1}H NMR measurements

The NMR measurements were made using an ELLAB TEL-Atomic PS 15 (operating at 25 MHz in temperatures from liquid nitrogen temperature up to room temperature) and Tecmag Scout (operating at 24.7 MHz at temperatures below liquid nitrogen) spectrometers. The spin–lattice relaxation times, T_1, were measured using a saturation sequence of π/2 pulses followed by a variable time interval τ and a reading π/2 pulse. The magnetisation was found to recover exponentially within experimental error at all temperatures. The temperature down to liquid nitrogen of the sample was controlled by a UNIPAN 660 temperature controller operating on Pt 100 sensor providing long time-temperature stability better than 1 K. Below temperatures of liquid nitrogen, and the helium-cooled Leybold cryostat was applied. The powder sample was evacuated at room temperature and then sealed under vacuum in a glass ampule. All measurements were made by heating the sample. The errors in the measurements of T_1 were estimated to be about 5%.

3. Results and discussion

3.1 UV-Vis spectroscopy

In solution, the degree of proton transfer from the donor to the acceptor can be simply determined by comparison of their pKa values. The proton resides typically on the molecule with the higher pKa value, but these values are mostly from aqueous solution, whereas the situations in the crystal are much more complicated. Although the difference in pKa [ΔpKa = pKa *base*-pKa *acid*] of the carboxylic acid and aromatic base may be a great indicator in order to determine, whether hydrogen bond is with, N^+–H···O^-, or without proton transfer, O–H···N. According to literature for complexes were ΔpKa<3.75 the neutral hydrogen bond should be formed, whereas ΔpKa>3.75 results in proton transfer[20,21]. In the case of the 66DMBP·CLA complex, ΔpKa equals 4.44, which means that the ionic salts should form in both polymorphic forms. The electronic structure of chloranilic acid is strongly susceptible to the conditions applied under experiments, as shown in Fig. 1a. The colour of the crystal is related to the degree of deprotonation of the acid molecule. The neutral acid (H_2CLA) is dark orange, the mono-anion ($HCLA^-$) is dark violet, and opaque and chloranilate dianions (CLA^{-2}) is also dark violet but more transparent[22]. Fig. 1b depicts the UV/VIS of two solutions: orange for α–66DMBP·CLA in acetone and dark violet for β–66DMBP·CLA in methanol. The peak for α–66DMBP·CLA is at 496 nm , and for β–form at 521 nm, this redshift proved that in the methanolic solution the chloranilic acid is mono deprotonated. It can suggest that in this solution, ionic pairs have been formed just before the crystallisation process. In contrast, in acetone, both acid and base molecules are probably neutral, and proton transfer takes place during crystallisation.

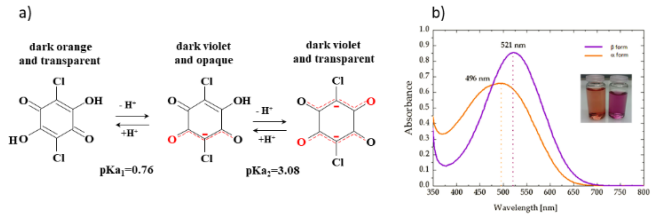

Fig. 1. a) Dissociation of chloranilic acid (H_2CLA) into the monoion ($HCLA^-$) and dianion (CLA^{2-}). The dashed lines indicate electron delocalisation in anions[22]. b) The UV/VIS diagrams for α–66DMBP·CLA and β–66DMBP·CLA in the acetone (dark orange) and methanol (violet), respectively

3.2 Computational Methods and Details

Static calculations

Calculations for neutral molecule (Fig. 2a) provides, regardless of the chemical surrounding, a value of Θ_{NCCN} = 180° for the most energetically favoured conformation, which is the *trans* form. Also, we have another minimum at about Θ_{NCCN} = 36°. Whereas for cation form (Fig. 2b) we observe, also regardless of the chemical surrounding, the global minimum for Θ_{NCCN} = 0° - *cis* form. These calculations also provide the information about conformational barriers, i.e. the amount of the energy required to change conformations from *trans* to *cis* or *cis* to *trans* for neutral or cationic form, respectively.

Table 1. The *trans/cis* energy barriers in different solvents for a neutral and cationic form of the 66DMBP molecule with different solvation models. All values are in kJ mol^{-1}.

solvent	*trans/cis* energy barriers for neutral 66DMBP [kcal·mol^{-1}/kJ·mol^{-1}]		*cis/trans* energy barriers for cationic $66DMBP^+$ [kcal·mol^{-1}/kJ·mol^{-1}]	
	PCM	COSMO	PCM	COSMO
acetone	5.6/23.4	4.7/19.66	8.6/36	7.8/32.5
ethanol	5.6/23.4	4.6/19.25	8.6/36	7.8/32.5
methanol	5.5/23.0	4.6/19.25	8.5/35.6	7.732.2

For both forms of 66DMBP, if we take solvent effects into account implicitly, and without any temperature effects, it seems that the only differences in relative energy are between molecules in the gas phase and in a solvent. However, in the experiment, we obtained two different forms in two different solvents, therefore the step forward into a more sophisticated approach must be made.

Dynamic calculations

Only dynamic calculations elucidated that solvent indeed has a huge impact not only on differences in free energies but also on preferred values of the dihedral angle. In the case of the neutral form (Fig. 3a), *trans* confirmation is still energetically preferred, but we observe different minima – for acetone 176° and methanol 163°. The *trans/cis* free energy barriers are 5.5 and 3.6 kcal·mol^{-1} for 66DMBP in acetone and methanol, respectively. While in a case of the cationic form (Fig. 3b) we can conclude that solvent has no impact on preferred values of dihedral angle (0°), but the *cis/trans* free energy barriers are 5.6 and 5.0 kcal mol^{-1} for acetone and methanol, respectively.

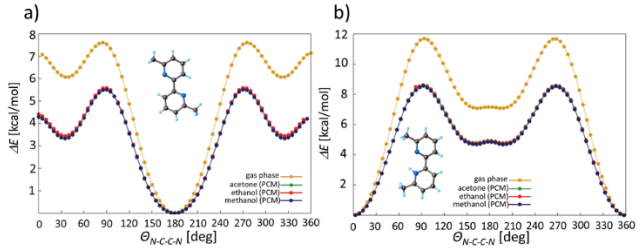

Fig. 2. Energy profiles along the dihedral angle N-C-C-N for the 6,6'-dimethyl-2,2'-bipyridinium (panel A) and N-protonated 6,6'-dimethyl-2,2'-bipyridinium cation (panel B) for the T = 0K case obtained by Gaussian09 with B3LYP/cc-pVTZ. Molecules are shown in insets Θ = 180° and Θ = 0° respectively). Gold points represent isolated molecule and green, red and blue points (curves) results from the Polarisable Continuum Model (PCM) for acetone, ethanol and methanol respectively.

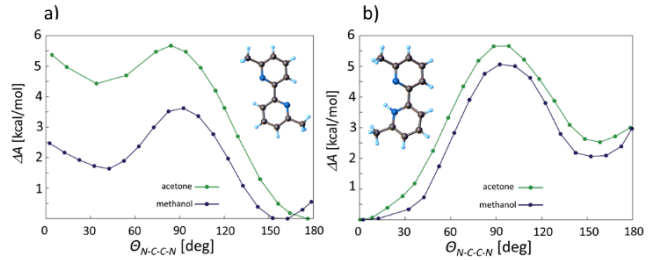

Fig. 3. Free energy profiles computed by means of the "blue moon" ensemble approach from ab initio molecular dynamics using the efficient Car-Parrinello propagation scheme at T = 295 K with explicit solvent for the 66DMBP (a) and N-protonated 66DMBP cation (b). The activation free energies were evaluated using the thermodynamic integration. Molecules are shown in insets (Θ_{NCCN} = 90°).

In this work to overcome the problem that standard AIMD cannot yet access the timescales required to observe the high energy processes since the thermal energy is typically much smaller than the energy barriers that separate two states we employ appropriate enhanced sampling ("rare event") techniques in conjunction with AIMD simulations. Specifically, we have used ab initio thermodynamic integration based on the so-called "blue moon" sampling.[23,24] The "blue moon" ensemble approach (also known as constrained reaction coordinate dynamics) is able to furnish a one–dimensional reaction profile along with the progress variable that has been chosen to drive the reaction of interest. Again, this technique can be applied together with AIMD simulations carried out with different solvents. The coordinate in all the molecular dynamics simulations performed in this work has been the dihedral angle N-C-C-N.

3.3 X-ray crystal structure analysis

The single-crystals of **1**–**3** were obtained by slow evaporation from the solution at constant temperatures and their structures were determined by an X-ray diffraction analysis. The asymmetric units, as well as the packing diagrams for the reported compounds, are presented in Fig. 4 and 5, respectively. The selected most important bond lengths and angles of **1**–**3** are collected in Tables S2-S4 (ESI). The hydrogen bond and π···π interaction parameters are listed in Table S5 (ESI).

1 adopts the $P2_1/c$ space group of the monoclinic system. The asymmetric unit of **1** contains one 66DMBP$^+$ and one BRA$^-$ in the cationic and anionic forms (1:1), respectively (see Fig 4a). In the **1**, one hydrogen atom from O5 atom (hydroxyl group) of the BRA is transferred to N11 atom of the 66DMBP. The proton transfer substantially shortens C5–O5 bond in the BRA$^-$ anion moiety from 1.327(4) to 1.232(4) Å and widens the C=N–C angle in 66DMBP$^+$ cation from 118.7(3) to 123.4(3)º for C26—N21—C22 and C16—N11—C12, respectively. Similar observations were present in the other bipyridyl derivatives with different methyl substituents.[5,25–28] The 66DMBP$^+$ cation adopts the *cisoid* arrangement.

Analysis of the packing and interaction in the crystal lattice of **1** reveals the presence of dimers assembled by O2–H2···N21 and N11–H11···O3 hydrogen bonds between the base and acid molecules (Fig. 4a). These interactions lead to the formations of the ring motifs that can be described by the $[R_2^2(10)]$ graph set notations.[29] Neighboring dimers are connected by hydrogen bonds (Table S5a, ESI) and π···π contacts (Fig. S3a, ESI).

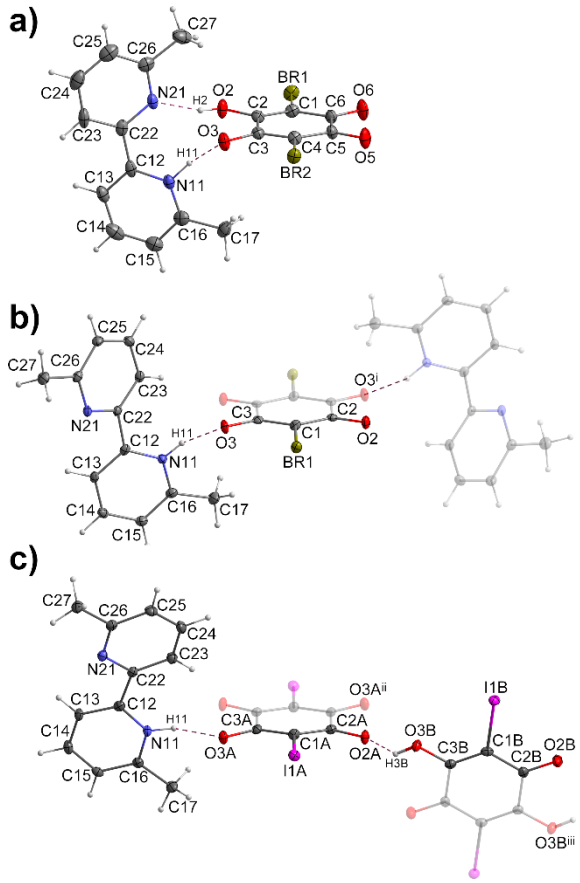

Fig. 4. The asymmetric unit of the a) **1** (66DMBP·BRA 1:1), b) **2** (66DMBP·BRA 2:1), and c) **3** (66DMBP·IA 1:1) crystal structure showing the atom-numbering scheme. Displacement ellipsoids are drawn at the 50% probability. Transparent part completes the chemical formula. Symmetry codes: (i) −*x*+1, −*y*, −*z*+2; (ii) −*x*+1, −*y*+1, −*z*+1; (iii) −*x*+2, −*y*+1, −*z*+2.

The **2** crystal crystallizes in the $P\bar{1}$ space group of the triclinic system. The unrelated part of the unit cell comprises the one 66DMBP^{+} cation and one-half BRA^{2-} dianion molecules (2:1), see Fig. 4b. The N11 and N21 atoms of the pyridyl rings around the central bond are to each other in *transoid* arrangement.

The crystal structure of **2** reveals double-proton transfer from hydroxyl groups (from atoms O3 and O3^{i}). This observation was confirmed by a detailed analysis of the bond length and angle values of the cation and dianion. According to these data, the double-proton transfer from the dianion to the cation are supported by the shortening of the C3–O3 and C3^{i}–O3^{i} to 1.250(3) Å. On the other hand, the protonation of nitrogen in the pyridyl ring widens the C12–N11–C16 angle from 118.1(2) to 123.5(2)º. Similar observations can be observed in the analogue with stoichiometry 1:1 (**1**). The 66DMBP^{+} and BRA^{2-} molecules are linked by strong and weak N–H···O hydrogen bonds (N11–H11···O3 2.665(3) Å and N11–H11···O2^{i} 3.099(3) Å, symmetry code is the same as in Table S5b). Additional stabilization of the crystal structure is by the other hydrogen bonds listed in Table S5b (ESI). Moreover, the analysis of the packing in the crystal lattice of **2** has not revealed the π···π-type contact (the distance between centroid-to-centroid of the pyridyl rings and dihedral angle between planes are too large ~4.5 Å and ~30º, respectively).

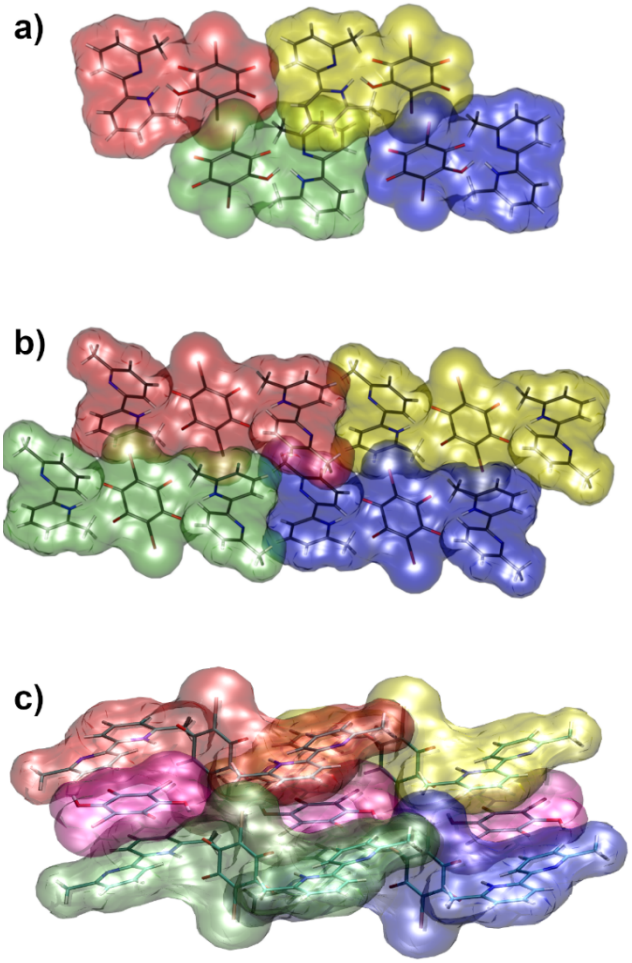

Fig. 5. Crystal packing of a) **1** (66DMBP·BRA 1:1), b) **2** (66DMBP·BRA 2:1) and c) **3** (66DMBP·IA 1:1). The drawings were made in the molecular graphics program VMD.[30]

The crystal **3** adopts the $P\bar{1}$ the space group of the triclinic system. The unrelated part of the unit cell with the atom-numbering scheme is presented in Fig. 4c. The asymmetric unit comprises the one 66DMBP^{+}, one-half IA^{2-} one-half IA in cation, dianion and neutral forms (2:1:1), respectively. Similar to the crystal **2,** in the crystal **3** the 66DMBP^{+} cation adopts the *trans* conformation.

In the crystal structure of **3,** two H atoms from the IA hydroxyl groups are transferred to nitrogen atoms in the aromatic rings of two 66DMBP molecules to form IA^{2-} dianion and two 66DMBP^{+} cations (2:1). The double proton transfer from hydroxyl groups in the IA^{2-} dianion (O3A and O3A^{ii} atoms) are corresponding with substantially shortening of the C3A–O3A and C3A^{ii}–O3A^{ii} bonds from 1.327(3) to 1.243(3) Å (comparison with neutral IA form of **3**, C3B–O3B bond length) and widening of the C=N–C angle in 66DMBP^{+} cation from 118.1(2) to 123.6(2)º.

The characteristic featured of **3** is the presence of the IA acid neutral form in the crystal lattice, which is placed between cation and dianion molecules. The analysis of the arrangement in the crystal lattice of **3** reveals the infinite H-bonded supramolecular chains between dianions and neutral forms of the IA acid (see Fig.

S4, ESI) comprising strong O–H···O contact (Table S5c). The other characteristic feature of this crystal is the formation of the π···π contact structure with non-aromatic–aromatic–aromatic–non-aromatic rings π-stacking interactions (see Figure S3b, Table S5c in ESI). The creating of π-stacking interactions between non-aromatic–aromatic rings were observed previously in quinones (and the other non-aromatic polyenic systems).[31]

3.4 Neutron scattering spectra

The molecules containing methyl groups show interesting properties at low temperature. The methyl groups do not jump over the barrier in a classical way, and their motions have to be described by the wavefunctions, including the tunnelling effects between potential minima.[32] As a consequence below ca. 50 K the so-called tunnelling peaks can appear, e.g. in the inelastic neutron scattering (INS) spectra of the compounds. The determination of the spectra parameters allows us to describe the dynamical behaviour of the methyl groups at these low temperatures. We can expect, for example, that the value of the transition energy between the ground and first exciting levels, E_{01}, for the CH_3 rotation could be a measure of the hydrogen bond strength in the molecular complexes, formed with the participation of bipyridyl and organic acids. In this paper, we present the INS spectra for the pure-66DMBP, **2** and **3** in the temperature region between 3 and 40 K corresponding to the tunnelling of the CH_3 groups. The tunnelling spectra at 4K for pure-66DMBP, **2** and **3** are depicted in Figs 5a-c. Tunnelling results at several temperatures in the energy range between ±10 and ±25 μeV for either pure-66DMBP or **2** and **3**, complexes are presented in Fig. S5 (ESI).

For pure-66DMBP one set of inelastic peaks has been found, whereas for the molecular complexes **2** and **3** there are two peaks on each side of the central elastic line. The energy of excitation between librational energy levels, E_{01}, was estimated based on the following equation:

$$\hbar\omega = \hbar\omega(\mathrm{T}=0)\left[1\text{-}\mathrm{A}^{\sin}\exp\left(\frac{E_{01}}{k\mathrm{T}}\right)\right] \qquad (1)$$

Where $\hbar\omega$ is the position of the peak, T is temperature and k – the Boltzmann constant, $\hbar\omega$(T=0) is the position of the peak extrapolated to T=0. The energy E_{01} represents the transition from the pocket groundstate to the first librational level. The sinusoidal coupling coefficient, A^{sin}, and the energy, E_{01}, describe the interaction between the methyl group and the heat bath. The position of the tunnelling peaks for 66DMBP and its complexes with either iodanilic or bromanilic acids as well as the corresponding energies of activation are presented in Table 2.

The fits were carried out with a standard model, consisting of a Dirac component for the elastic scattering, and Lorentzian for the tunnelling excitations (shown as solid green and blue lines in Figs. 6a-c). The theoretical curves are convoluted with the instrumental resolution function obtained during the present experiment for vanadium (red lines). Figs. S6a-c (ESI) show the Arrhenius plot related to the positions of the 1-1', and 2-2' peaks in the temperature range 3-40 K, for which the tunnelling peaks could be observed. The estimated values of the excitation energy measured for the peaks assigned as 1-1' equal to 17, 16 and 16.1 meV for pure-66DMBP, **2** and **3**, respectively. In the case of peaks 2-2' the estimated energies are smaller (13.7 for **2** and 12.2 meV for **3**) compared to those measured for the peaks 1-1'. Observed energy values are typical for this type of compounds and similar to the dependence of the energy value on the position of the peak in relation to the elastic one observed previously.[5,33]

In order to discuss the INS tunnelling spectra of pure-66DMBP, **2** and **3** it is necessary to know a number of independent methyl groups in the crystal structure. When we take into account, for example, another organic molecule called TAAD (p-*N*,*N*'-tetraacetylodiaminoduren), we can expect eight independent methyl groups, i.e. eight peaks on one and the other side of the central peak.

Table 2. Tunnelling energies (μeV) for the 6-6'-dimethyl-2,2'-bipyridyl and its complexes with either chloranilic, bromanilic or iodanilic acids at 4 K and corresponding energies of activation estimated according to Eq. (1).

compounds	peak position [μeV]		E_{01} [meV]	
	1-1'	2-2'	1-1'	2-2'
pure-66DMBP	±1.4	-	17	-
66DMBP·BRA (2:1), **2**	±2.1	±3.5	16	13.7
66DMBP·IA (1:1), **3**	±1.02	±7.6	16.1	12.2
α–66DMBP·CLA	only QENS:100-200 K			
β–66DMBP·CLA	not observed			

As was presented in ref.[34], only two pairs of the peak with different intensity were observed during neutron scattering. The detailed structural analysis, either hydrogen bonds or short contacts, in which the methyl groups were involved, showed that the groups were inequivalent. It was suggested that the observed effects are results of two interplaying contributions: the crystal packing and specific interaction of the hydrogen bond type. Following this path, we can discuss the INS spectra in the case of 66DMBP complexes. The 66DMBP base molecule possesses two methyl groups in the structure, and it means that we should observe at most two pair of peaks in the INS spectra. According to the crystal data, pure-66DMBP, which was determined at 150 K, crystallises in the space group $P2_1/c$, and the molecules are lying on a centre of symmetry, creating the *transoid* arrangement.[35] The observation of one pair of the inelastic peaks (see Fig. 6a), suggests that pure base has the same structure at 4 K as at 150 K and both methyl groups are equivalent.

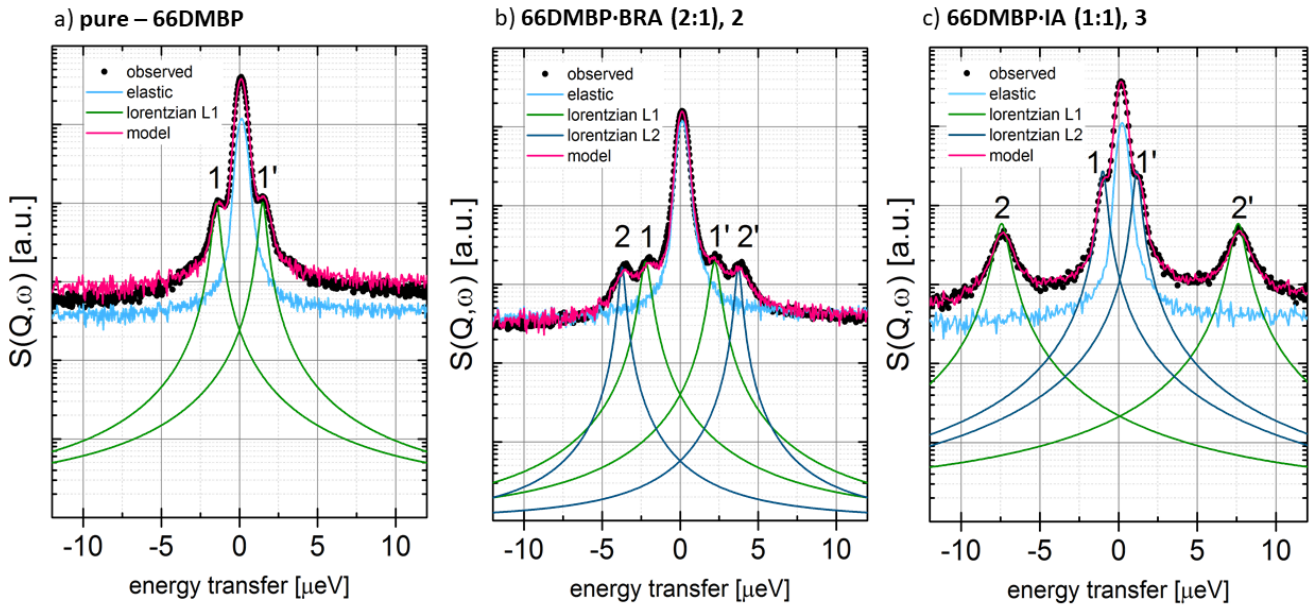

Fig. 6. The INS spectra at 4 K for a) pure - 66DMBP, b) **2**, 66DMBP·BRA (2:1) and c) **3**, 66DMBP·IA. The Lorentzians taken for convolution are shown in green, the elastic contribution in blue, the model after the convolution - in red.

When we look more closely at the structural data presented above, we will note that the methyl group tunnelling signals are observed only for *trans* conformation of the base molecules. In the case of compound **1**, the base molecule adopts the *cisoid* arrangement. The *cis* conformation results in an unconventional interaction between hydrogens from the methyl group and acceptors. Based on Table S5 (ESI), in the crystal, two weak hydrogen bonds (C17···O5^{iii} and C27···O6^{V}) reduce the lability of the methyl groups. The structure for β–66DMBP·CLA, is isostructural with that of the compound **1**. For the *cisoid* arrangement of the base molecule for β–66DMBP·CLA, no inelastic tunnelling has been observed within the accessible energy range (see Fig. S7b, ESI)

In the molecular complexes of **2** and **3**, two signals in Figs. 5c and 5d should be the results of the presence of two independent methyl groups. From the crystallographic data at 100 K and under the assumption that there is no phase transition at low temperature we know that the 66DMBP molecules occupy a general position (both for **2** and **3**) in the structure, so the two CH_3 groups may be treated as independent.

The *transoid* arrangement in the base molecule, which is mono-protonated, makes that each methyl group has different environments and interactions. The methyl group labelled as C17 possesses the protonated nitrogen atom (N11-H11), group C27, in contrast, is adjacent to a nitrogen atom not bound by any interaction with the other moieties.

In the case of **2** as well as **3** one peak (1-1') is close to the elastic line and the second one is in a position relatively distant to the central one. According to the hydrogen-bond geometry included in Table S5 (ESI), the C17 methyl group is stabilised by one short contact: C17-H17*B*···Br1^{ii} (3.895(3)Å and 156°) and C17—H17*A*···O2*A*^{ii} (3.228(3) Å and 125°), for **2** and **3**, respectively. In both crystals, the C27 group exhibits relatively large freedom for rotation due to the lack of any interaction between this group and the hydrogen acceptors. Based on this analysis, the 1-1' peak can be assigned to the C17 group, while the 2-2' one to the C27 group.

In the case α–66DMBP·CLA only QENS signal was recorded for a temperature range between 50 and 150K (Fig. S7a, ESI), no tunnelling peaks at 3 K were found. The QENS spectra were analysed by using a function consisting of one elastic and one quasielastic component. The elastic scattering of neutrons is due to the atoms, which move too slowly to be resolved with the resolution of the instrument and move in a stochastic manner. Whereas, the quasielastic component expresses the energy transfer, gain and loss, due to the hydrogen motions.[36,37] The dynamic structure factor S(Q, ω) is given by equation (2):

$$S(\omega, Q)=R(\omega, Q)\otimes(A_0\delta(\omega)+A_1(Q)L_1(\omega))+B(Q) \quad (2)$$

$$L_1(\omega)=\frac{1}{\pi}\frac{\Gamma}{\Gamma^2+\omega^2} \quad (3)$$

where R(ω, Q) is the instrumental resolution, δ(ω) is a Dirac delta function, $L_1(\omega)$ is a Lorentzian function defined by equation (3) and Γ is the bandwidth parameter (Half-Width at Half Maximum, HWHM). The B(Q) part describes the flat inelastic background in the QENS region.

The experimental data were evaluated in two ways. First, the data were analysed for detectors binned over a Q range of 0.6-1.66 $Å^{-1}$. This procedure is only reasonable if the half widths, Γ, are mainly independent of Q, which is fulfilled for the presented investigations (see Fig. S8 in ESI). For the thermally activated process, the temperature dependence of Γ is expected to obey an Arrhenius equation:

$$\Gamma = \Gamma_\infty \exp\left(-\frac{E_a}{kT}\right) \quad (4)$$

where E_a is the activation energy for the rotation and Γ_∞ is related to the attempt frequency. Based on this data, the activation energy was obtained from the slope in Fig. 7a, and equals to 50.6 meV (4.85 kJ/mol) and $\Gamma_\infty = 1.0$ meV. Here, the activation energy is a measure of the barrier for the classical hopping between adjacent wells, defined as the difference between the top of the barrier and the ground state in the methyl group rotation. The calculated value of E_a is consistent with the typical activation energies of the methyl rotations (a few tens of meV).[38–40]

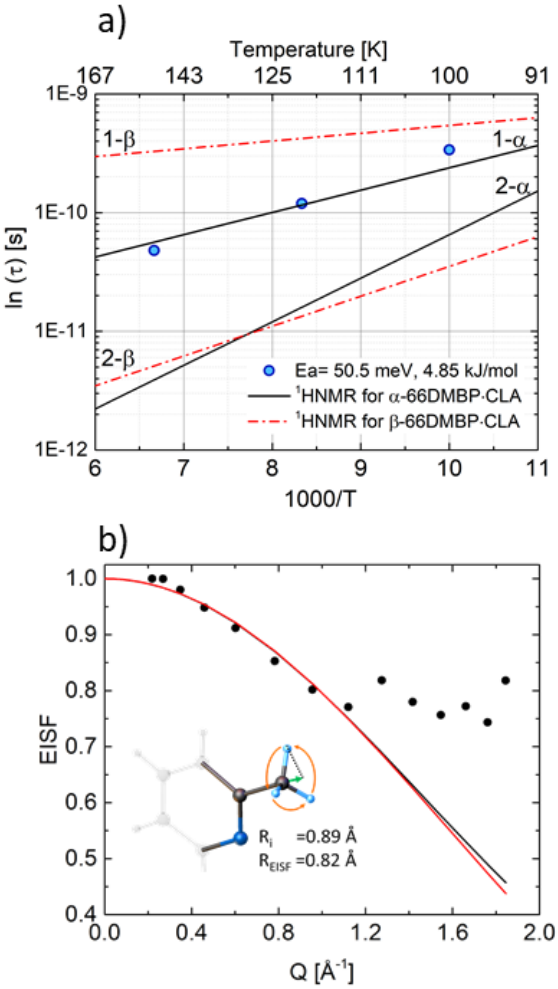

Fig. 7. a) The correlation time obtained from NMR measurements (black and red lines) and QENS (blue points). b) Experimental EISF of α–66DMBP·CLA measured at 100 K. The black line describes the 3-site rotation of the methyl group, whereas the red line the isotropic free rotation.

In the second approach, the experimental data were evaluated for each detector of the SPHERES spectrometer. In order to examine the geometry of the methyl rotational motions, we computed the elastic incoherent structure factor (EISF) as the ratio:

$$\text{EISF} = \frac{A_0(Q)}{A_0(Q) + A_1(Q)} \quad (5)$$

where the intensity A_0 and A_1 corresponded to purely elastic and quasielastic scattering, respectively. Fig. 7b presents the experimental points of the EISF in dependence of Q, and two possible modes of the rotation received during the fitting.

Here we can consider only two physically reasonable models for the methyl group CH_3 namely: (1) threefold reorientational jumps of CH_3 around C-CH_3 (around C_3 axis) or (2) isotropic free CH_3 rotation.

For the first model, the EISF is $\frac{1}{3}\left[1+2j_0(\sqrt{3}QR)\right]$ for the second model EISF=$j_0^2(QR)$ describes the free rotation of the methyl group around C-CH_3. In this equation, j_0 denotes the spherical Bessel function of zeroth order, R the distance of the protons to the 3-fold symmetry axis, *Q* the momentum transfer. These two models describe the motion with the same radii, R_i =0.895 Å, which can be calculated based on the X-ray data as a distance from the hydrogen atom to the C_3 axis.[6] Based on EISF data, the theoretical R_{EISF} equals to 0.82 Å. The average time between three successive reorientational jumps around the C_3 axis can be calculated from the following formula: $\tau_3 = 3\hbar/2\Gamma$.[36,37] For the investigated samples, the fitted mean time between jumps, τ, changes from $4.8\cdot10^{-11}$ (150 K) to $3.4\cdot10^{-10}$ s (100 K).

2.5 ^{1}H NMR measurements

The temperature dependencies measured of the ^{1}H NMR spin–lattice relaxation time (T_1) in the temperature range between 20 and 320 K for studied compounds,α–66DMBP·CLA and β–66DMBP·CLA, are shown in Fig. 8.

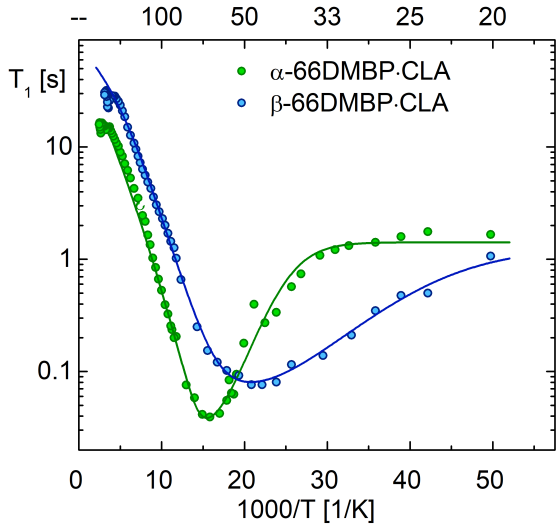

Fig. 8. The temperature dependence of the proton spin-lattice

relaxation time, T_1, measured at 25 MHz.

For α–66DMBP·CLA the temperature dependence of the spin–lattice relaxation time has two distinct ranges. For temperatures below 31 K, the relaxation times are nearly constant (1.3 ÷ 1.7 s) that means (in the absence of possible tunnelling of the methyl groups) that the interaction of protons with close quadrupolar halogen atoms (chloride) plays the dominating mechanism of the spin relaxation. Above 31 K the wide (with different slopes) minimum with T_{1min} = 40 ms at 63K, is visible. In the case of β–66DMBP·CLA, in the low temperature region, the flattening is not fully shaped. One, rather wide minimum with T_{1min} = 74 ms at 48 K with more distinctly different slopes is present. At the highest temperatures (320 K), the spin–lattice relaxation times of both samples reaches 16 and 32 s for α–66DMBP·CLA and β–66DMBP·CLA, respectively. The complete relaxation for both studied compounds consists of two relaxation mechanisms: one is attributed to the interaction between hydrogen and quadrupole nuclei (low temperature flattening), and the second to the classical ^{1}H–^{1}H dipole-dipole interactions (relaxation minimum at high temperatures). It should be noted that the different slopes of the T_1 minimum also originate from an inequivalency of two methyl groups, significantly spaced apart in the 66DMBP molecule. Therefore we fit the temperature dependence of the T_1 relaxation time using the sum of three components in the whole temperature range.[41–46]

$$\frac{1}{T_1} = C_1\left[\frac{\tau_c}{1+\omega_H^2\tau_{ci}^2}+\frac{4\tau_c}{1+4\omega_H^2\tau_c^2}\right] + C_2\left[\frac{\tau_c}{1+\omega_H^2\tau_{ci}^2}+\frac{4\tau_c}{1+4\omega_H^2\tau_c^2}\right] + C_{HCl}\left[\frac{\tau_{c,Q}}{1+\left(\omega_H-\omega_Q\right)^2\tau_{c,Q}^2} + \frac{3\tau_{c,Q}}{1+4\omega_H^2\tau_{c,Q}^2}+\frac{6\tau_{c,Q}}{1+\left(\omega_H+\omega_Q\right)^2\tau_{c,Q}^2}\right] \quad (6)$$

If we look at the previously presented results regarding tunnelling of methyl groups[5,47–49], we can draw the following conclusions. The value of the activation energy, E_{01}, which described the first librational transition, strongly depends on the inelastic peak's position ($\hbar\omega$) relative to elastic one. The resulting relationship is that the higher value of the tunnelling transition the higher E_{01} value. This effect, in our opinion, affects the value of activation energy, E_a, in the classic terms. Assuming two independent methyl groups in the molecules, and based on the data from Table 2, the relaxation time τ_i is presented for each group, named as 1,2-α and 1,2-β for α–66DMBP·CLA and β–66DMBP·CLA, respectively. In the case of α–66DMBP·CLA, we have found an excellent consistency between the results obtained from QENS and ^{1}H NMR for one methyl group, denoted as 1-α. The motions describe as 2-α (the second methyl group for the α form) have not been revealed in the INS spectra recorded using the SPHERES spectrometer within the available time window (~100 ps to 3 ns).

Based on X-ray data presented in ref.[5,6], we assume that methyl group C6 (Fig S1a in ESI) has a different environment than C6'. In its surroundings the nitrogen atom from the aromatic ring is protonated, this group is also associated with two unconventional interactions: C-H···O and C- H···Cl. In contrast, the C6 'methyl group is involved only in one hydrogen bond (C-H···O). Therefore its rotational movement should be more free. Therefore, C6' methyl group is assigned as 1-α, and C6 as 1-β.

Table 2. Activation energies, correlation times and motional constants evaluated for α–66DMBP·CLA and β–66DMBP·CLA for the temperature dependence of T_1. The notations 1,2 - α, β correspond to the number of methyl group in α–66DMBP·CLA and β–66DMBP·CLA (consistent with those in Fig. 7a)..

parameters	α–66DMBP·CLA	β–66DMBP·CLA
CH_3 (1)	1 - α	1 - β
E_a[meV]	3.60	1.26
τ_0 [s]	$3.15\ 10^{-12}$	$1.2\ 10^{-10}$
C [s^{-2}]	$9.6\ 10^{9}$	$1.9\ 10^{8}$
CH_3 (2)	2 - α	2 - β
E_a[meV]	7.03	4.81
τ_0 [s]	$1.39\ 10^{-14}$	$1.08\ 10^{-13}$
C [s^{-2}]	$9.6\ 10^{9}$	$1.9\ 10^{8}$

4. Conclusion

In this paper, pure base 66DMBP, and its complexes with anilic acids have been studied by the method sensitive to the molecular dynamics, in particular to the proton motion in the hydrogen bonds in the infinite chains of the HBs as well as in the specific motifs (dimers, trimers). From the symmetry of the crystal structure also it may result that the methyl groups become different, especially at low temperatures. One tunneling peak is observed for the pure 66DMP base in the INS spectra at low temperature. In turn we have found two tunneling peaks for the following molecular complexes: **2**: 66DMBP·BRA (2:1), **3**: 66DMBP·IA (1:1), which indicates two crystallographically independent methyl groups in their crystal structures. It should be, however, emphasised that the differentiation of the methyl groups may appear due to two effects: the crystal packing and possible proton transfer in the hydrogen bonds. We have estimated the parameters of the CH_3 tunnelling observed in the INS spectra at low temperature. The estimated values of the energy of excitation between librational energy levels, E_{01}, are rather typical as for this type of compounds.

In the case of a *cisoid* arrangement, no additional peak (inelastic in the INS sectra) has been observed in the vicinity of the elastic one for β–66DMBP·CLA. In the case of the 66DMBP molecule, the methyl groups are substituted in the aromatic ring at the 6,6' positions. Therefore, the *cis* conformation facilitates to form the unconventional C-H···X interaction. Moreover, the QENS signal is observed for the α–66DMBP·CLA form as well. The fitting procedure applied for QENS indicates the classical methyl group

rotations (3-site model) above 50 K. The model is supported by the NMR results.

Based on our calculations, we can conclude that in order to elucidate the real effects of the solvent on the crystallization of a compound, we must use more sophisticated methods such as *ab initio* molecular dynamics, simulations, where not only specific interactions between solute and solvent molecules but also the temperature effects are taken into account. Also, we can preliminarily propose a general mechanism of the formation of the α and β forms of the 66DMBP·CLA complex, based on the calculations and UV-VIS spectra. Since in both forms, we have N-protonated 66DMBP, but in different conformations, *trans* and *cis,* respectively, we suggest that the proton transfer in the α form takes place during crystallization, whereas in the β form - already in the solution. Nevertheless, to verify our predictions and unravel detailed mechanisms, some more advanced and computationally demanding calculations are needed.

Conflicts of interest

There are no conflicts to declare.

Acknowledgments

M. R. gratefully acknowledge the financial support provided by JCNS to perform the neutron scattering measurements at the Heinz Maier-Leibnitz Zentrum (MLZ), Garching, Germany.

P. D. would like to gratefully acknowledge the Wroclaw Centre for Networking and Supercomputing (WCSS) for the allocation of computer time on the BEM Cluster.

The authors (M.R., M.M., and G. B.) gratefully acknowledge the financial support provided by the National Science Center of Poland, No. UMO-2016/21//ST3/004640201/2078/17

P.D. gratefully acknowledges financial support from the National Science Centre of Poland (2016/23/B/ST4/01099)

Notes and references

1 C. Blanchet-Boiteux, P. Friant-Michel, A. Marsura, J.-B. Regnouf-de-Vains and M. F. Ruiz-López, Theoretical study of solvent effects on the conformational equilibrium and electronic spectra of 2,2′-bipyridine derivatives*, J. Mol. Struct. THEOCHEM*, 2007, **811**, 169–174.

2 J. Kalenik and Z. Pawełka, Solvent influence on conformational equilibrium in 3-nitrobenzaldehyde, *J. Mol. Liq.*, 2005, **121**, 63–68.

3 S. Horiuchi, R. Kumai and Y. Tokura, High-temperature and pressure-induced ferroelectricity in hydrogen-bonded supramolecular crystals of anilic acids and 2,3-Di(2-pyridinyl)pyrazine, *J. Am. Chem. Soc.*, 2013, **135**, 4492–4500.

4 R. Kumai, S. Horiuchi, J. Fujioka and Y. Tokura, Ferroelectricity and pressure-induced phenomena driven by neutral ionic valence instability of acid-base supramolecules, *J. Am. Chem. Soc.*, 2012, **134**, 1036–1046.

5 G. Bator, W. Sawka-Dobrowolska, L. Sobczyk, E. Grech, J. Nowicka-Scheibe, A. Pawlukojć, J. Wuttke, J. Baran and M. Owczarek, 4,4′-, 5,5′-, and 6,6′- dimethyl-2,2′-bipyridyls: The structures, phase transitions, vibrations, and methyl group tunneling of their complexes with chloranilic acid, *J. Chem. Phys.*, 2011, **135**, 044509-1–12.

6 K. Kobayashi, S. Horiuchi, S. Ishibashi, F. Kagawa, Y. Murakami and R. Kumai, Structure-property relationship of supramolecular ferroelectric [H-66dmbp][Hca] accompanied by high polarization, competing structural phases, and polymorphs*, Chem. - A Eur. J.*, 2014, **20**, 17515–17522.

7 H. A. Torrey and W. H. Hunter, The action of iodides on bromanil. Iodanil and some of its derivatives*, J. Am. Chem. Soc.*, 1912, **34**, 702–716.

8 G. M. Sheldrick, A short history of SHELX*, Acta Crystallogr. Sect. A Found. Crystallogr.*, 2007, **64**, 112–122.

9 G. M. Sheldrick, Crystal structure refinement with SHELXL*, Acta Crystallogr. Sect. C Struct. Chem.*, 2015, **71**, 3–8.

10 CrysAlis CCD and CrysAlis PRO, Agilent Technologies, 1.171.37.35.

11 S. Miertuš and J. Tomasi, Approximate evaluations of the electrostatic free energy and internal energy changes in solution processes*, Chem. Phys.*, 1982, **65**, 239–245.

12 S. Miertuš, E. Scrocco and J. Tomasi, Electrostatic interaction of a solute with a continuum. A direct utilizaion of AB initio molecular potentials for the prevision of solvent effects, *Chem. Phys.*, 1981, **55**, 117–129.

13 S. Sinnecker, A. Rajendran, A. Klamt, M. Diedenhofen and F. Neese, Calculation of solvent shifts on electronic g-tensors with the conductor-like screening model (COSMO) and its self-consistent generalization to real solvents (direct COSMO-RS), *J. Phys. Chem. A*, 2006, **110**, 2235–2245.

14 T. H. Dunning, Gaussian basis sets for use in correlated molecular calculations. I. The atoms boron through neon and hydrogen, *J. Chem. Phys.*, 1989, **90**, 1007–1023.

15 D. Marx and J. Hutter, Ab initio molecular dynamics: basic theory and advanced methods, *Cambridge Univ. Press*, 2009.

16 R. Car and M. Parrinello, Unified Approach for Molecular Dynamics and Density-Functional Theory*, Phys. Rev. Lett.*, 1985, **55**, 2471–2474.

17 J. Wuttke, A. Budwig, M. Drochner, H. Kämmerling, F. Kayser, H. Kleines, V. Ossovyi, L. C. Pardo, M. Prager, D. Richter, G. J. Schneider, H. Schneider and S. Staringer, SPHERES , Jülich ' s high-flux neutron backscattering spectrometer at FRM II SPHERES , Jülich ' s high-flux neutron backscattering spectrometer at FRM II, *Rev. Sci. Instrum. Suppl. Mat.*, , DOI:10.1063/1.4732806.

18 J. Wuttke, SLAW--- a neutron histogram to scattering law converter, http://apps.jcns.fz-juelich.de/slaw.

19 J. Wuttke, FRIDA --- Flexible rapid interactive data analysis, http://apps.jcns.fz-juelich.de/frida.

20 S. L. Johnson and K. A. Rumon, Infrared Spectra of Solid 1:1 Pyridine-Benzoic Acid Complexes; the Nature of the Hydrogen Bond as a Function of the Acid-Base Levels in the Complex*, J. Phys. Chem.*, 1965, **69**, 74–86.

21 P. H. Stahl and C. G. Wermuth, *Handbook of pharmaceutical salts: properties, selection, and use*, VHCA;

Wiley-VCH: Weinheim, New York, 2002.
22 K. Molanov and B. Kojić-Prodić, Salts and co-crystals of chloranilic acid with organic bases: Is it possible to predict a salt formation?, *CrystEngComm*, 2010, **12**, 925–939.
23 E. A. Carter, G. Ciccotti, J. T. Hynes and R. Kapral, Constrained reaction coordinate dynamics for the simulation of rare events, *Chem. Phys. Lett.*, 1989, **156**, 472–477.
24 M. Sprik and G. Ciccotti, Free energy from constrained molecular dynamics, *J. Chem. Phys.*, 1998, **109**, 7737–7744.
25 M. Rok, P. Szklarz, M. Moskwa, M. Kijewska, J. Baran, G. Bator, W. Medycki and M. Zamponi, Structures and phase transitions in neat 4,4′-di-: Tert -butyl-2,2′-bipyridyl and in its molecular complexes with either bromanilic or iodanilic acid, *CrystEngComm*, 2017, **19**, 6883–6895.
26 S. Horiuchi, R. Kumai and Y. Tokura, High-temperature and pressure-induced ferroelectricity in hydrogen-bonded supramolecular crystals of anilic acids and 2,3-Di(2-pyridinyl)pyrazine, *J. Am. Chem. Soc.*, 2013, **135**, 4492–4500.
27 S. Horiuchi, R. Kumai and Y. Tokura, A supramolecular ferroelectric realized by collective proton transfer, *Angew. Chemie - Int. Ed.*, 2007, **46**, 3497–3501.
28 R. Kumai, S. Horiuchi, Y. Okimoto and Y. Tokura, Large dielectric susceptibility associated with proton transfer in a supramolecular structure of chloranilic acid and 5,5[sup ′]-dimethyl-2,2[sup ′]-bipyridine, *J. Chem. Phys.*, 2006, **125**, 084715-5.
29 M. C. Etter, Encoding and Decoding Hydrogen-Bond Patterns of Organic Compounds, *Acc. Chem. Res.*, 1990, **23**, 120–126.
30 W. Humphrey, A. Dalke and K. Schulten, VMD: Visual Molecular Dynamics, *J. Mol. Graph.*, 1996, **14**, 33–38.
31 K. Molcanov and B. Kojić-Prodić, Towards understanding π-stacking interactions between non-Aromatic rings, *IUCrJ*, 2019, **6**, 156–166.
32 M. Prager and A. Heidemann, Rotational tunneling and neutron spectroscopy: A compilation, *Chem. Rev.*, 1997, **97**, 2933–2966.
33 M. Rok, G. Bator, W. Sawka-Dobrowolska, P. Durlak, M. Moskwa, W. Medycki, L. Sobczyk and M. Zamponi, Crystal structural analysis of methyl-substituted pyrazines with anilic acids: A combined diffraction, inelastic neutron scattering,1H-NMR study and theoretical approach, *CrystEngComm*, 2018, **20**, 2016–2028.
34 G. Bator, M. Rok, W. Sawka-Dobrowolska, L. Sobczyk, M. Zamponi and A. Pawlukojć, P-N,N′-tetraacetylodiaminodurene. the structure and vibrational spectra, *Chem. Phys.*, 2015, **459**, 148–154.
35 A. Sengül, M. B. Hursthouse, S. J. Coles and R. D. Gillard, 6,6′-Dimethyl-2,2′-bipyridyl*, Acta Crystallogr. Sect. C Cryst. Struct. Commun.*, 1998, **54**, 661–662.
36 M. Bee, *Quasielastic Neutron Scatering*, Adam Hilger, Bristol and Philadelphia, 1988.
37 D. Blanchard, J. B. Maronsson, M. D. Riktor, J. Kheres, D. Sveinbjörnsson, E. Gil Bardají, A. Léon, F. Juranyi, J. Wuttke, K. Lefmann, B. C. Hauback, M. Fichtner and T. Vegge, Hindered rotational energy barriers of BH4- tetrahedra in β-$Mg(BH_4)_2$ from quasielastic neutron scattering and DFT calculations, *J. Phys. Chem. C*, 2012, **116**, 2013–2023.
38 A. Pajzderska, M. A. Gonzales, J. P. Embs, J. Mielcarek, and J. W. Wąsicki, Dynamics of an amorphous pharmacologically active compound – diazepam : a QENS study combined with molecular dynamics simulations, *RSC Adv.*, 2017, **7**, 35504–35515.
39 A. M. A. Leguy, J. M. Frost, A. P. McMahon, V. G. Sakai, W. Kochelmann, C. Law, X. Li, F. Foglia, A. Walsh, B. C. O'Regan, J. Nelson, J. T. Cabral and P. R. F. Barnes, The dynamics of methylammonium ions in hybrid organic-inorganic perovskite solar cells, *Nat. Commun.*, 2015, **6**, 1–10.
40 M. Kofu, M. Tyagi, Y. Inamura, K. Miyazaki and O. Yamamuro, Quasielastic neutron scattering studies on glass-forming ionic liquids with imidazolium cations, *J. Chem. Phys.*, 2015, **143**, 234502-1–10.
41 D. Kruk, A. Privalov, W. Medycki, C. Uniszkiewicz, W. Masierak and R. Jakubas, *NMR Studies of Solid-State Dynamics*, Elsevier Ltd., 1st edn., 2012, vol. 76.
42 A. Piecha, R. Jakubas, A. Pietraszko, J. Baran, W. Medycki and D. Kruk, Structural characterization, thermal, dielectric, vibrational properties and molecular motions in $[C_3N_2H_5]_6[Bi_4Br_{18}]$, *J. Solid State Chem.*, 2009, **182**, 2949–2960.
43 J. Przesławski, W. Medycki, A. Piecha, R. Jakubas and D. Kruk, Dynamics and ferroelectric phase transition of $(C_3N_2H_5)_5Bi_2Br_{11}$ by means of ac calorimetry and 1H NMR relaxometry, *Chem. Phys.*, 2013, **410**, 19–24.
44 M. Węcławik, P. Szklarz, W. Medycki, R. Janicki, A. Piecha-Bisiorek, P. Zieliński and R. Jakubas, Unprecedented transformation of $[I^-{\cdot}I_3^-]$ to $[I_4^{2-}]$ polyiodides in the solid state: Structures, phase transitions and characterization of dipyrazolium iodide triiodide, *Dalton Trans.*, 2015, **44**, 18447–18458.
45 A. Piecha-Bisiorek, R. Jakubas, W. Medycki, M. Florek-Wojciechowska, M. Wojciechowski and D. Kruk, Dynamics of Ferroelectric Bis (imidazolium) Pentachloroantimonate (III) by Means of Nuclear Magnetic Resonance 1H Relaxometry and Dielectric Spectroscopy, *J. Phys. Chem. A*, 2014, **118**, 3564–3571.
46 D. Kruk, W. Medycki, A. Mielczarek, R. Jakubas and C. Uniszkiewicz, Complex Nuclear Relaxation Processes in Guanidinium Compounds $[C(NH_2)_3]_3Sb_2X_9$(X = Br, Cl): Effects of Quadrupolar Interactions, *Appl. Magn. Reson.*, 2010, **39**, 233–249.
47 A. Piecha-Bisiorek, G. Bator, W. Sawka-Dobrowolska, L. Sobczyk, M. Rok, W. Medycki and G. J. Schneider, *J. Phys. Chem. A*, Structure and tunneling splitting spectra of methyl groups of tetramethylpyrazine in complexes with chloranilic and bromanilic acids, *J. Phys. Chem. A*, 2014, **118**, 7159−7166.
48 W. Sawka-Dobrowolska, G. Bator, L. Sobczyk, E. Grech, J. Nowicka-Scheibe and A. Pawlukojć, Structure and vibrational spectra of 1:1 Chloranilic Acid (CLA) - Tetramethylpyrazine (TMP) complex, *Struct. Chem.*, 2005, **16**, 281–286.
49 G. Bator and L. Sobczyk, H-bonded complexes between pyrazines containing methyl groups and strong proton donors : structure and dynamics, *Trends in Organic Chemistry*, 2014, **17**, 93–105.